Derya Aksu Demirezen*, Şeyda Yılmaz, Dilek Demirezen Yılmaz and Yalçın Şevki Yıldız

Green synthesis of iron oxide nanoparticles using *Ceratonia siliqua L.* aqueous extract: improvement of colloidal stability by optimizing synthesis parameters, and evaluation of antibacterial activity against Gram-positive and Gram-negative bacteria

https://doi.org/10.1515/ijmr-2022-0037
Received January 31, 2022; accepted May 19, 2022;
published online September 13, 2022

Abstract: This study focused on the colloidal stability enhancement of iron oxide nanoparticles synthesized using aqueous extract of the *Ceratonia siliqua L.* (carob pod) by optimizing the synthesis parameters. The synthesis parameters were determined as the concentration of iron ions, the concentration of extract, *pH* of extract, temperature, stirring rate, and reaction time. The significance of the studied factors in controlling the particle size distribution of nanoparticles was quantitatively evaluated via analysis of variance (ANOVA). Iron oxide nanoparticles were produced with an average zeta potential of +41 ± 0.8 mV, hydrodynamic size of 78 ± 22 nm, and a polydispersity value of 0.42 ± 0.06, respectively. As a result of the stability study by measuring the zeta potential, it was determined that the colloidal stability was maintained for 3 months. Green iron oxide nanoparticles (gIONPs) showed inhibition zones of 24.27 ± 0.12 mm and 20.83 ± 0.11 mm in 250 mg/mL concentration against Gram-negative (*Escherichia coli*) and Gram-positive (*Staphylococcus aureus*) bacterial strains, respectively. *S. aureus* was susceptible to the gIONPs according to the standard antibiotics of Cefotaxime (≥23 mm), Tetracycline (≥19 mm), Gentamicin (≥15 mm), and Cefoxitin (≥22 mm). *E. coli* was susceptible to the gIONPs according to the standard antibiotics of Tetracycline (≥19 mm) and Gentamicin (≥15 mm), but showed resistance to the Cefotaxime (15–22 mm) and Cefoxitin (≤21 mm) standard antibiotics. This study suggests that the green synthesized iron oxide nanoparticles could be used as an antimicrobial agent and a promising candidate for usage in sensor, biomedical, and electronics applications for being in a highly stable structure.

Keywords: Antibacterial activity; Green synthesis; Iron oxide nanoparticles; Process optimization; Stability.

1 Introduction

Nanoparticles have been prepared through a diverse range of synthesis approaches over the last decades and different fundamental principles of synthesis procedures have been investigated to obtain nanoparticles of desired sizes, shapes, and functionalities. The unique size-dependent thermal, electrical, chemical and optical properties have enabled their use in fields such as medicine and chemical analysis [1].

The green synthesis approach is a promising synthesis procedure in the research and development of materials science and technology due to the biosynthetic pathway of nanoparticle preparation, potentially eliminating the usage of hazardous chemicals and making the nanoparticles more biocompatible. Some basic principles of "green synthesis" can be explained by the prevention or minimization of waste, reduction of pollutant derivatives, and the use of safer solvents as well as renewable feedstock [2]. The biomaterials extracted from several parts of the plant are mixed with metal precursor solutions under different reaction conditions for nanoparticle synthesis. The biomaterials play several roles such as reducing, capping, and stabilizing agents in the nanoparticle synthesis process. Nanoparticles are synthesized within a few minutes or hours depending upon the type and concentration of biochemicals arising from plant sources. The plant extracts have been proven to possess high efficiency as stabilizing and reducing agents for the synthesis of nanoparticles but

***Corresponding author: Derya Aksu Demirezen**, Graduate School of Natural and Applied Sciences, Erciyes University, 38280, Talas, Kayseri, Turkey, E-mail: dademirezen@gmail.com.
https://orcid.org/0000-0002-1979-9903
Şeyda Yılmaz, Graduate School of Natural and Applied Sciences, Erciyes University, 38280, Talas, Kayseri, Turkey; and NanoBiotech, Erciyes Teknopark, Tekno-2, 38039, Melikgazi, Kayseri, Turkey
Dilek Demirezen Yılmaz, Department of Biology, Faculty of Sciences, Erciyes University, 38280, Talas, Kayseri, Turkey; and NanoBiotech, Erciyes Teknopark, Tekno-2, 38039, Melikgazi, Kayseri, Turkey
Yalçın Şevki Yıldız, Department of Environmental Engineering, Faculty of Engineering, Erciyes University, 38280, Talas, Kayseri, Turkey

a detailed investigation of the role of reaction parameters in synthesis is still needed to overcome existing problems in "green" synthesis [3].

Several parameters affect the green synthesis of nanoparticles, including *pH* of the solution, temperature, the concentration of the plant material used, reaction time, and above all the protocols that are used for the synthesis process. The change in the type and characteristic of the synthesized nanoparticles is especially affected by the type of plant material used in the synthesis process [4]. The morphology and surface chemistry of nanoparticles are important parameters for their applications. An ideal synthesis method should be able to allow reliable adjustment of particle distribution, size, and composition [5]. Capping agents significantly modify the properties of colloidal suspensions of nanoparticles. The efficacy of colloidal NPs application is linked to high suspension stability and zeta potential is a good indicator of the stability of the nanoparticles. Small changes to the solution (e.g., background salt concentration, temperature, *pH*), or changes to the nanoparticles (e.g., surface coating or concentration) can substantially affect stability. The better antibacterial action may be attributed to their smaller size and surface charge to come in contact with the microbial cells [6].

There are different phases of iron oxides: hematite (α-Fe_2O_3), maghemite (γ-Fe_2O_3), goethite (α-FeOOH), and magnetite (Fe_3O_4). The size scale affects these materials' optical, electrical, and biocompatibility properties [7, 8]. The functional groups of coating materials alter the surface charge, which influences the biological behavior of iron oxide nanoparticles [9]. The dispersity, size, and surface chemistry of the iron oxide materials are crucial for environmental applications in the aqueous phase due to the porous structure with particle–surface interaction [10]. Iron oxide nanoparticles act as promising antibacterial agents with high surface areas with crystalline morphologies at a high number of edges and corners and generate oxidative stress by reactive oxygen species [11].

In this study, we report in highly stable iron oxide nanoparticles synthesized using biochemicals extracted from *Ceratonia siliqua. L.* (carob pod). Carob pod is rich in sugars such as sucrose (437.3 mg/g dry weight), glucose (395.8 mg/g dry weight), and fructose (42.3 mg/g dry weight). The other content consists of the total phenolics group (13.51 mg gallic acid equivalents [GAE]/g dry weight), proanthocyanidins (0.36 mg GAE/g dry weight), gallotannins (0.41 catechin equivalents [CE]/g dry weight), and flavonols (3.21 mg CE/g dry weight protein). Gallic acid (3.27 mg/g dry weight) is the most abundant phenolic material. Aspartic acid (18.25 mg/g dry weight protein) is the predominant amino acid in the protein fraction. Major minerals are vitamin K, calcium, potassium, and magnesium [12].

The effects of synthesis parameters on the dimensions and dispersity of iron oxide nanoparticles were investigated by the Taguchi method. The Taguchi method is used for evaluating the results of matrix experiments to determine the best levels of experimental parameters. It makes it possible to provide an acceptable formulation using minimum raw materials and time [13]. The signal-to-noise (S/N) ratio and the analysis of variance (ANOVA) were employed to analyze the experimental parameters. The synthesis parameters including the concentration of plant extract, the concentration of iron ion, reaction temperature, *pH* of plant extract, stirring rate, and reaction time were evaluated. After each synthesis, the polydispersity value of nanoparticles was measured by a dynamic light scattering (DLS) instrument to analyze the effect of the chosen experimental parameters. The zeta potential and UV–Vis spectrum were monitored over 3 months period for analysis of colloidal stability.

The aqueous extract of the *C. siliqua L.* (carob pod) has been used as a reducing, capping, and stabilizing agent for the gIONPs synthesis in our previous studies [14]. However, the stability of gIONPs obtained from the previous procedure by the aqueous extract of the *C. siliqua L.* (carob pod) was poor with a zeta value of +22.2 mV [15]. In this study; the synthesis parameters of gIONPs production using an aqueous extract of *C. siliqua L.* (carob pod) were optimized for the first time to obtain a stable monodisperse colloidal solution. By obtaining a homogeneous iron oxide nanoparticle colloidal dispersion solution, the stability of the nanoparticles in terms of zeta value was obtained at $+41 \pm 0.8$ mV and preserved for 3 months [16].

There are several studies about the potency of green nanomaterials for usage as a better substitute for conventional antibacterial drugs due to their simple, cost-effective, and eco-friendly synthesis procedures. Some of these antibacterial studies were related to iron oxide nanoparticles by *Moringa oleifera* leaf extract [17], iron oxide nanoparticles by *Acorus calamus* extract [18], copper oxide nanoparticles by *Zea mays L.* dry husk extract [19], silver nanoparticles by extract of *Gongronema Latifolium* [20], silver nanoparticles by using bitter leaves (*Veronica amygdalina*) extract [21]. Therefore, the antibacterial activity of powder gIONPs synthesized from the aqueous extract of the *C. siliqua L.* (carob pod) was tested against

Gram-negative *Escherichia coli* (*E. coli*) and Gram-positive *Staphylococcus aureus* (*S. aureus*) bacteria to assess the efficacy at the biological interface.

2 Experimental procedure

2.1 Materials

The carob pod was purchased from the local market in Kayseri, Turkey. Ferric chloride ($FeCl_3{\cdot}6H_2O$), sodium hydroxide (NaOH), and hydrochloric acid (HCl) were purchased from Merck. Ultrapure water was used in the experiments (Elga Purelab Option-Q 7).

2.2 Synthesis and characterization of gIONPs

The method for the extraction of the carob pod used was similar to the procedure followed in our previous study [22]. 10 g of carob pod pieces were extracted in 150 mL of ultrapure water for 2 h. The resultant extract was filtered through Whatman No.1 filter paper and was used as a reducing and capping agent for the green synthesis of iron oxide nanoparticles. 3.8 g of ferric chloride ($FeCl_3.6H_2O$) was dissolved in 100 mL of ultrapure water for 15 min. The extract to precursor iron solution was mixed at a 1:1 vol ratio. The addition of the plant extract to ferric chloride aqueous solution led to turning the initially yellowish solution to a brown color indicating the formation of iron oxide nanoparticles. The resultant colloidal nanoparticle solution was stirred for 3 h and kept in a +4 °C refrigerator to do stability analysis. Nanoparticles were precipitated by adjusting the *pH* value of gIONPs colloidal solution to 7.2 and the pellet was washed with ultrapure water and ethanol twice. It was dried in a laboratory oven at 70 °C for 10 h. The brownish–black powder of gIONPs (Figure S1) was used for characterization and antibacterial analysis.

The characterization of the gIONPs was achieved using X-ray powder diffraction (XRD Bruker AXS D8), Scanning electron microscopy (SEM) with energy dispersive X-ray (EDX) mapping (SEM – LEO 440), and Fourier-transform infrared spectroscopy (FTIR Perkin Elmer 400). Instrumental analysis was performed by the Nanotechnology Research Center (ERNAM) and Technology Research Center (TAUM), Erciyes University. Transmission electron microscopy (TEM) images were recorded using the JEOL 1220 JEM TEM of the Eskişehir Osmangazi University Research Laboratory Application and Research Center (ARUM). The size and dispersity of nanoparticles were analyzed using a dynamic light scattering (DLS) instrument (Horiba nanoPartica SZ-100V2), NanoBiotech Research Laboratory.

The average crystallite size of gIONPs was determined using Debye–Scherrer equation $d = (k\lambda/\beta\cos\theta)$, where k is the Debye–Scherrer constant (0.94 for FWHM of spherical crystals with cubic symmetry), λ is the X-ray wavelength (0.154 nm), β is the width of the peak with the maximum intensity in half-height, d is the thickness of the crystal, and θ is the diffraction angle (radian). Origin 2021b (© 1991–2021 OriginLab Corporation) was used for the calculation of the FWHM of XRD peaks for the calculation of β.

2.3 Design of experiment and analysis

In this study, the design of experiment (DOE) strategy and the Taguchi method for the experimental design approach was used to find optimum experimental conditions of the gIONPs with the minimum polydispersity index value (*PDI*). The goal was the investigation of the six parameters of synthesis including temperature (Temp), *pH* of carob pod extract, extract concentration of carob pod, the concentration of iron ion, stirring rate (rpm), and reaction time (time). Six experimental parameters used for the green synthesis of iron oxide nanoparticles and their corresponding three levels are given in Table 1. The analysis of variance (ANOVA) was used to determine the significance of individual parameters for the control of the final response.

The *S*/*N* ratio and the analysis of variance (ANOVA) with a significance level of 0.05 were employed to study the contributions of the parameters to the response. The Minitab software version 13 (Ankara, Turkey) is a tool for the statistical design of experiments that were used. The equivalent volume of the gIONPs suspension (2 mL) was diluted with a constant volume (2 mL) of deionized

Table 1: Experimental parameters for gIONPs and corresponding levels.

Parameters	Levels		
	Low	Center	High
The *pH* of carob pod extract	5.00	8.00	11.00
Temperature (°C)	25.00	55.00	85.00
Carob pod extract concentration (% mg/mg)	5.00	10.00	20.00
The concentration of iron ion (M)	0.07	0.14	0.28
Stirring rate (rpm)	200	400	600
Reaction time (h)	1.00	2.00	3.00

water and then subsequently all measurements were performed at room temperature at the DLS instrument. The experiments of 27 runs with 3 trials were conducted for three levels of six parameters.

2.4 Stability analysis of gIONPs

The zeta potential measurement of the colloidal gIONPs samples was determined using a zeta potential analyzer (Horiba nanoPartica SZ-100V2). The method used by the SZ-100V2 is known as laser Doppler electrophoresis. The sample was irradiated with a laser light of 532 nm at 3.3 electrode voltage. A cell with an electrode was used to introduce an electric field into the sample. All presented zeta potentials were reported as the mean value of three independent measurements at 25 °C temperature. UV–Visible spectroscopy (Hach DR 6000 UV—Vis spectrophotometer) was used for monitoring the maximum absorbance of nanoparticles over time. The UV—Vis spectrum of the gIONPs sample at a dilution ratio of 1:10 (v/v) was monitored using a 1 cm glass cuvette. The absorbance spectrum was obtained between 200 and 700 nm. The stability analysis was performed for 3 months.

2.5 Antibacterial activity analysis of gIONPs by the well-diffusion method

The bacterial culture and antibiotic discs were obtained from the Veterinary Medicine Faculty Laboratory of Erciyes University. The bacterial activity of gIONPs was assessed against both Gram-negative (*E. coli 0157:H7*) and Gram-positive (*S. aureus ATCC 25923*). The antibacterial activity analysis was performed using to the Kirby—Bauer well diffusion method. Briefly, the selected bacterial pathogenic strains were subcultured on Mueller–Hinton nutrient broth and the turbidity of the culture was made equivalent to 0.5 McFarland standards (1×10^8 CFU mL^{-1}). Each strain was spread uniformly on nutrient agar plates using a sterile cotton swab. A sterile cork borer was used to create a well of about 8 mm diameter for testing the antibacterial activity of gIONPs. 250 mg of gIONPs was mixed in 1 mL of water and the mixture was vigorously agitated on a mechanical vortex mixer before use. 100 µL of gIONPs was loaded into the well (8 mm diameter) on the Mueller—Hinton agar plate. Antibiotics of Cefoxitin (30 µg/disc), Cefotaxime (30 µg/disc), Gentamicin (10 µg/disc), and Tetracycline (30 µg/disc) were used as a positive control. The extract of *C. siliqua L.* (carob pod) (100 µL) was used as a negative control. Then the plates were incubated at 37 °C for 24 h.

The different zone levels of inhibition were measured and analyzed according to the Kirby–Bauer Interpretation chart (Table S3). The average values of triplicate measurements were calculated as an outcome of antibacterial activity.

3 Results and discussion

3.1 Optimization of gIONPs synthesis parameters

Taguchi's experimental design was employed based on the L27 orthogonal array for three levels of six parameters. The goal was the investigation of the six parameters of synthesis including the concentration of carob pod extract, the concentration of iron ion, temperature, *pH* of carob pod extract, reaction time, and stirring rate. Supplementary Table S1 shows the 27 experimental runs with their responses of hydrodynamic size and polydispersity (*PDI*) value according to the DLS measurements. A monodisperse suspension of nanoparticles contains particles of nearly the same size, whereas a polydisperse suspension contains particles of different sizes. The numerical value of *PDI* ranges from 0.0 (perfectly uniform sample) to 1.0 (multiple particle size populations) and is measured by the dynamic light scattering (DLS) technique [23]. The polydisperse nanoparticle solution is unstable and tends to agglomerate with time. The Brownian motion of the nanoparticles fortifies the stability of a colloidal system, which avoids precipitation and agglomeration. This motion improves with reduced particle size [24].

The *S*/*N* ratio results of each parameter effect on the *PDI* of gIONPs are presented in Figure 1 as graphs. The highest *S*/*N* ratios were selected for the smallest *PDI* value response. The response table for the *S*/*N* ratios of parameters is shown in Table 2. According to their larger value of delta, the parameters were assigned ranks 1, 2, 3, 4, 5, and 6. Rank 1 means the highest contribution parameter for the lowest *PDI* value while rank 6 means the lowest contribution parameter.

The reaction time is the highest contribution parameter while the *pH* of the carob pod extract is the least contribution parameter. The optimum parameter levels for the smallest *PDI* value were determined as 0.14 M iron ion concentration, 10 % extract concentration, extract *pH* of 5, 25 °C temperature, stirring rate of 400 rpm, and reaction time of 3 h (Figure 1). Plant extract is the dominant parameter in nanoparticle synthesis, as it is the source of reducing agents and stabilizing molecules. Increasing the plant concentration from 10 % to 20 % (w/w) increased the *PDI* of the nanoparticles, while also causing agglomeration

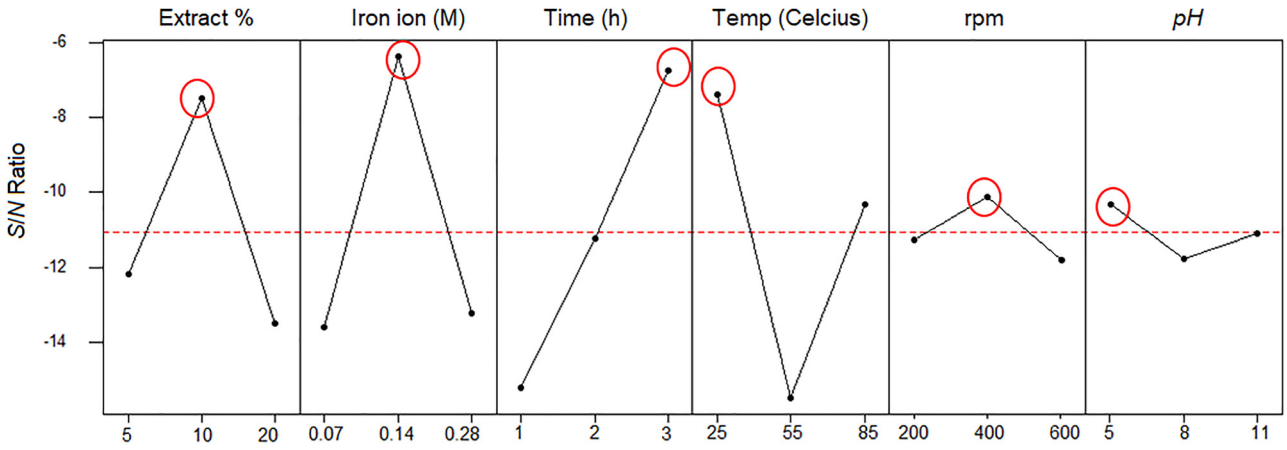

Figure 1: Main effects plot of *S*/*N* ratio for smallest PDI value.

Table 2: Response table for *S*/*N* ratios of PDI.

Level	Extract concentration	Iron ion	Time	Temp	rpm	*pH*
1	−12.1849	−13.5807	−15.2026	−7.3956	−11.2539	−10.3223
2	−7.4894	−6.3857	−11.2326	−15.4661	−10.1172	−11.7674
3	−13.4986	−13.2065	−6.7376	−10.3112	−11.8017	−11.0831
Delta	6.0092	7.1950	8.4651	8.0705	1.6846	1.4451
Rank	**Rank 4**	**Rank 3**	**Rank 1**	**Rank 2**	**Rank 5**	**Rank 6**

at 30 %. Meanwhile, enhancement of the reaction time from 1 to 3 h leads to nanoparticles with the smallest size. The stirring rate and *pH* of carob pod extract did not make a huge difference to the response. The direct effect of temperature may be due to enhancing the rate of nanoparticle formation [25]. The *pH* change at the carob pod extract might not have altered the electrical charges of biomolecules and capping agents and their ability to bind and reduce metal ions [26]. The stirring rate of 400 rpm was observed as a transition condition between the stirring rate of 200 and 600 rpm for the smallest size and polydispersity index. The low stirring rate was proved unable to produce iron oxide nanoparticles. The high mixing rate might have caused the nanoparticles to have high surface energy and caused their agglomeration [27]. Analysis of variance (ANOVA) showed the significance level of the studied parameters (Table 3). The results indicate that iron ion concentration, reaction time, temperature, and carob pod extract concentration had a significant effect on *PDI* value (p-value < 0.05).

There are several studies about the procedure optimization of the green synthesis of several nanoparticles such as silver, zinc, gold, etc. in the literature. The green synthesis of nanoparticles is related to various factors, including types of plant biomolecules and concentration, *pH*, temperature, stirring rate, and exposure time. These factors are found to control the sizes and morphologies of the nanoparticles according to the literature [28–31]. The effects of various parameters in the green synthesis method of iron nanoparticles such as iron precursor, plant extract concentration, reaction temperature, and *pH* have been little studied when the studies in the literature are reviewed. Kheshtzar et al. [32] reported that the quantity of leaf extract and concentration of iron precursor are the most effective parameters in the green synthesis reaction. It was revealed by Gholami et al. [33] that the iron precursor to extract ratio has a significant effect on green iron nanoparticle synthesis.

3.2 Characterization of gIONPs at optimum synthesis parameters

A follow-up characterization analysis was carried out considering the optimum values of synthesis parameters for gIONPs. The hydrodynamic size and *PDI* value of gIONPs at the optimum parameters were measured as 78 ± 22 nm and 0.42 ± 0.06, respectively (Figure 2a). gIONPs sample was measured at an average zeta potential of + 41 ± 0.8 mV (Figure 2b). The stability of nanoparticle solutions can be predicted by zeta potential measurements. The particles tend to agglomerate as the electric potential approaches zero. Particles tend to repel other particles at

Table 3: The results of ANOVA for the designed orthogonal array design in the optimization of gIONPs synthesis parameters.

Analysis of variance (ANOVA)					
Parameters	***DF***	**Adj *SS***	**Adj *MS***	***F*-Value**	***p*-Value**
Extract concentration (w/w %)	2	5.310	5.310	5.15	**0.021**
Iron ion (M)	2	28.023	28.023	27.18	**0.000**
Time (h)	2	37.887	37.887	36.75	**0.000**
Temp (°C)	2	46.776	46.776	45.37	**0.000**
rpm	2	1.921	1.921	1.86	**0.192**
pH of extract	2	2.410	2.410	2.34	**0.133**
Error	14	7.216	7.216		
Total	26	129.543			

DF: degrees of freedom; Adj *SS:* Adjusted sums of squares; Adj *MS:* Adjusted mean squares; *F*-value: value on the *F* distribution; *p*-Value: probability of obtaining test results.

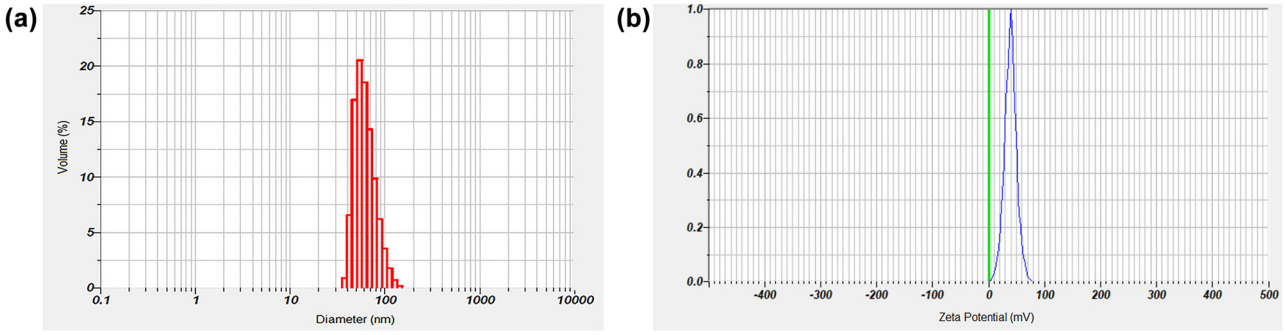

Figure 2: (a) The particle size distribution and (b) zeta potential of colloidal gIONPs.

the zeta potential of either more than +20 mV or less than −20 mV [34].

The formation of gIONPs in the aqueous colloidal solution was confirmed by the peak at 299 nm using UV–visible spectral analysis (Figure 3). As per the previously reported literature, this is due to the green biosynthesis of iron oxide nanoparticles [35]. The absorbance peak of iron oxide nanoparticles synthesized using plant extract ranged from 240 to 360 nm [36, 37]. The X-ray diffraction of gIONPs was recorded at 2θ values ranging from 10° to 80° (Figure 4). The XRD pattern showed distinct peaks at 24.20° (0 1 2), 33.18° (1 0 4), 35.68° (1 1 0), 40.90° (1 1 3), 49.54° (0 2 4), 54.17° (1 1 6), 62.47° (2 1 4), and 64.12° (3 0 0), which indicates the crystalline nature of the iron oxide nanoparticles and corresponds to the hematite (JCPDS No. 013–0534) [38, 39]. The average crystallite size of the nanoparticles was calculated as 5.09 nm using the Debye Scherrer equation.

SEM analysis was performed to evaluate the surface morphology of the gIONPs. Figure 5a reveals that the morphology of the nanoparticles is mostly in sphere form. The gIONPs tend to agglomerate according to the SEM image and this agglomeration may be due to the Van der Waals forces between particles or due to the solution form of the sample and improper drying [40, 41]. Figure 5b and c presents the images of iron oxide nanoparticles captured by TEM. The TEM images showed that the nanoparticles are spherical and some of the particles were agglomerated. In the absence of coating materials, iron oxide nanoparticles that form part of a colloid tend to agglomerate. These agglomerates may be caused by either strong or weak physical interactions [42].

The gIONPs at optimum conditions were also characterized by means of EDX to examine their composition. EDX was built in the microscope by which the SEM image of the sample was recorded. The EDX spectrum is presented in Figure S2. The atomic percentages are 33.14 % of oxygen and 64.26 % of iron. The EDX confirmed the presence of both iron and oxygen which indicates the reduction of iron ions to iron oxide by carob pod extract. The Cl signal was detected originating from iron chloride precursor salt used in the synthesis protocol and from the plant biomaterial used for the synthesis of nanoparticles. Signals for K were observed which may originate from the plant biomaterial [43].

FTIR spectroscopy for the extract and gIONPs solution was carried out. It was observed that the soluble elements present in plant extract acted as capping agents of gIONPs.

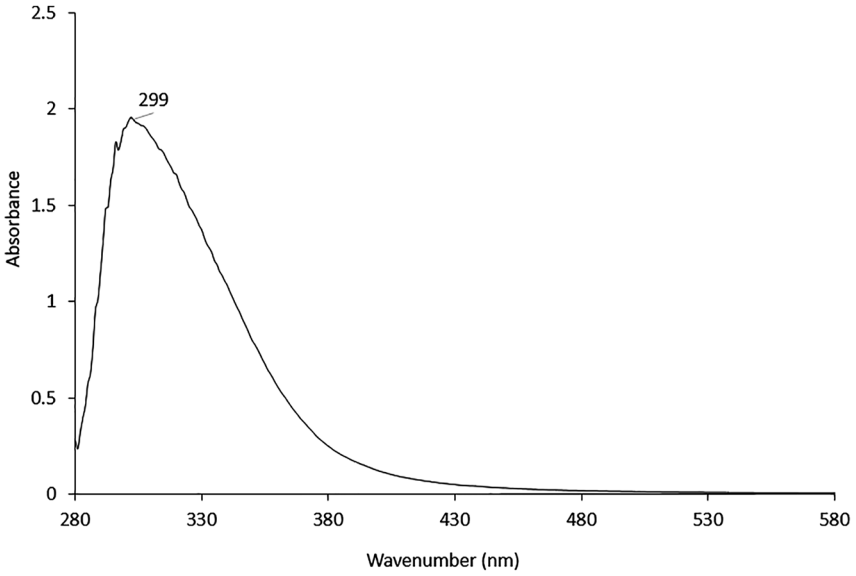

Figure 3: UV–Vis absorption spectrum of colloidal gIONPs.

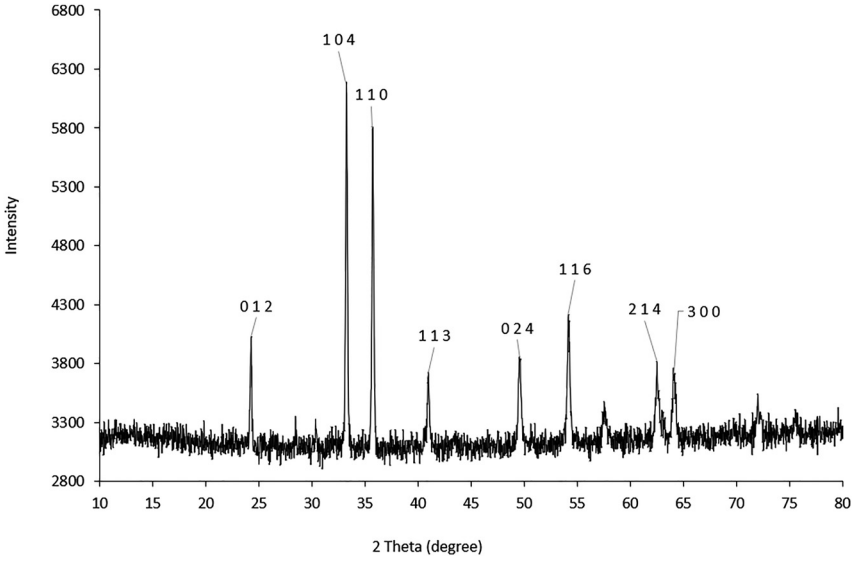

Figure 4: XRD pattern of gIONPs.

The spectra of the carob pod extract revealed absorption bands at 3493, 3120, 1708, 1377, 1040, 803, and 626 cm^{-1}, while the absorption bands of synthesized gIONPs were observed at 3028, 2080, 1680, 1390, 1047, 917, and 470 cm^{-1} (Figure 6).

The band at 3493 cm^{-1} is an indicator of stretching in the OH group within free hydroxyl [44]. The band located at 3120 cm^{-1} is assigned to stretching of O–H group bond in galactose sugar compound in carob pod extract [45]. The band in 1708 cm^{-1} shows the presence of unsaturated carbonyl groups [46]. The band in 1377 cm^{-1} is attributed to the symmetrical stretch of the methyl functional group [47]. The band at 1040 cm^{-1} can be assigned to the stretching vibration of C–N function groups in plant polyphenolic species [48]. The band in 626 cm^{-1} shows the C–S stretching [49]. The band at 3028 cm^{-1} is attributed to the C–H and C–O bending and stretching of oleic acids [50]. The band at 2080 cm^{-1} is also a typical band of stretching bands of unbound CO [51]. The absorption bands at 1047, 1680, and 1390 cm^{-1} were assigned to the strong C=O stretching band related to the carbonyl group and medium C–H bending, respectively [52]. The band at 917 cm^{-1} is attributed to the C–H bending due to the carbohydrate. The formation of gIONPs is characterized by the absorption bands from

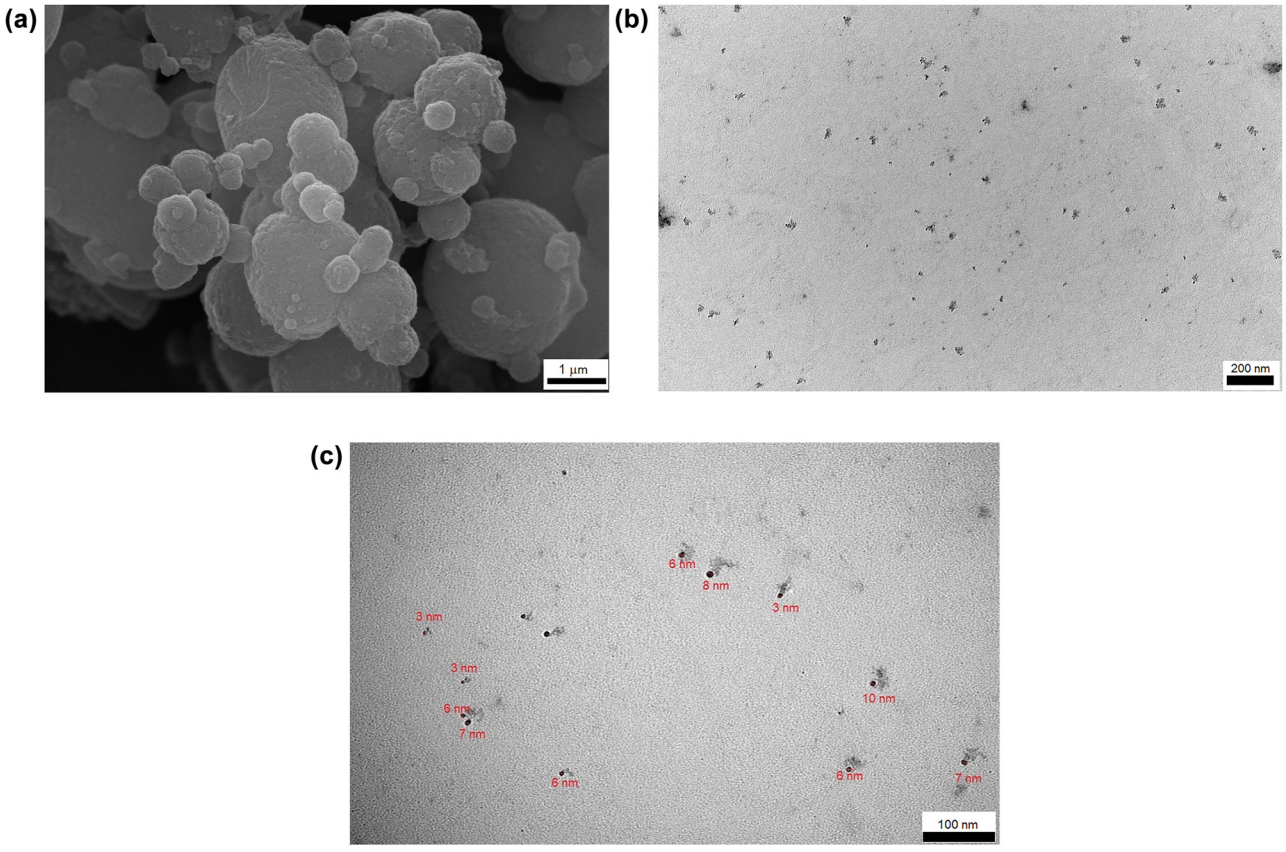

Figure 5: (a) SEM image and TEM images, (b) distribution, and (c) size and shape of gIONPs.

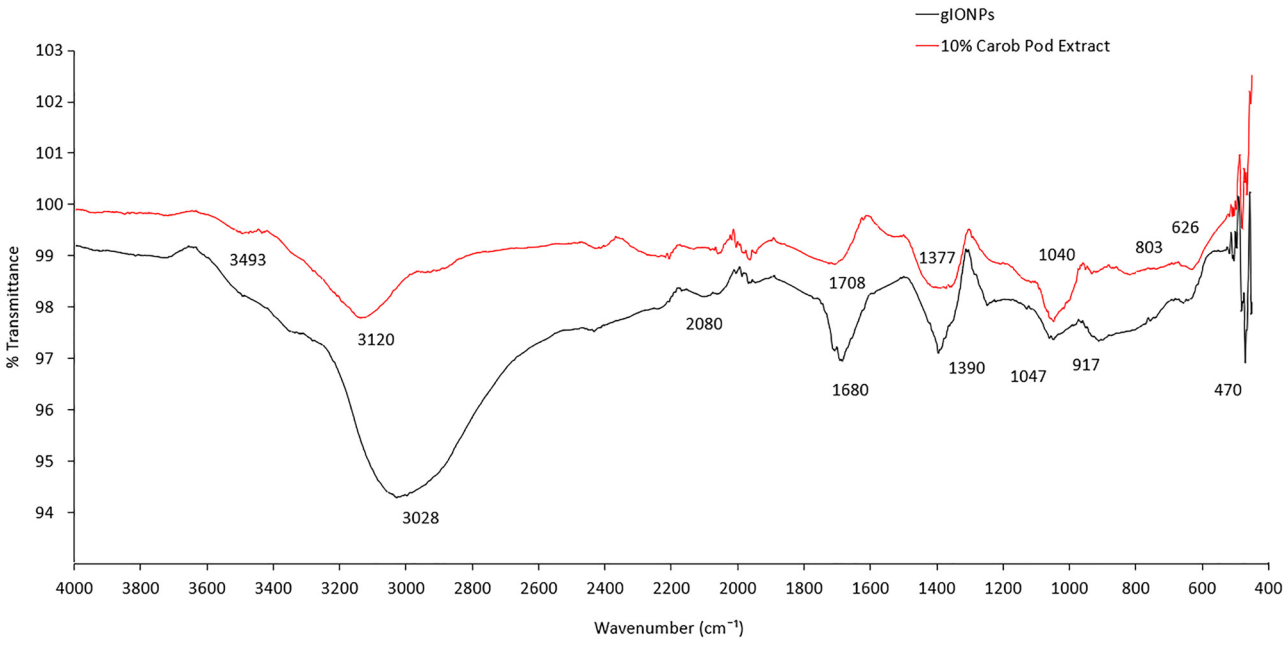

Figure 6: FTIR spectra of colloidal gIONPs and carob pod extract.

428 to 686 cm^{-1}. The band at 470 cm^{-1} corresponds to the Fe–O vibration bonds related to the octahedral units of the magnetite phase [53, 54]. This band was absent in plant extract which indicates the formation of iron oxide nanoparticles. A similar observation has been reported by several studies [55, 56].

3.3 Stability analysis of colloidal gIONPs at optimum synthesis parameters

The *pH* and zeta potential of colloidal gIONPs solution was measured as 1.9 and + 42.5 mV after synthesis, respectively. The schematic representation of zeta potential is seen in Figure S3. The good stability of gIONPs is defined by their high electrostatic potential (>40 mV) [57]. The stability of the colloidal gIONPs solution was evaluated by monitoring the zeta potentials over 3 months (Table 4). The zeta value had been measured as +22.2 mV according to the procedure used in our previous studies [58]. The colloidal stability of gIONPs was improved and maintained for 3 months at +41 ± 0.8 mV after the synthesis parameters optimization.

A similar study has been performed for the iron oxide nanoparticles synthesized using the aqueous coprecipitation method and it was observed that the zeta potential of nanoparticles was constant at around −39 mV for long-term storage (over 16 months) [59].

Table 4: Zeta potential measurement of gIONPs nanoparticles over 3 months.

Time (month)	Zeta potential (mV)	*pH*
0	+42.5	1.92
1	+41.0	1.91
2	+40.4	1.95
3	+40.8	1.90

The UV–Vis absorbance spectrum of gIONPs colloidal solution over 3 months was monitored and the maximum absorbance did not change during this period (Figure 7). Metal nanoparticles exhibit surface plasmon resonance (SPR) absorption dependent on the size, shape, and composition [60]. According to this phenomenon, it could be explained that gIONPs were formed with good stability and the composition did not change due to the formation of agglomerates during the 3 months [61]. Shoaib et al. have carried out similar stability experiments with green silver nanoparticles using UV–Vis spectroscopy and they indicated the change of the maximum absorbance due to the presence of agglomerations [62].

The *pH* of the isoelectric point of the gIONPs was determined as 6.8 by the zeta potential measurements (Figure 8a). The gIONPs began to agglomerate at *pH* values greater than 5 and less than 11 (Figure 8b).

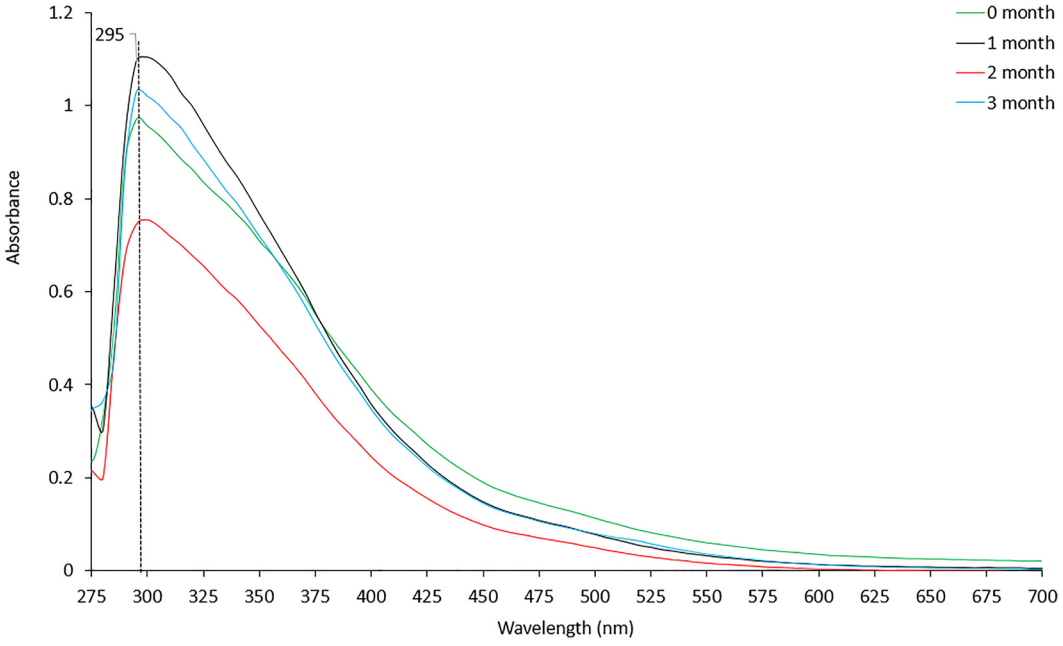

Figure 7: UV–Vis absorption spectra of colloidal gIONPs over 3 months.

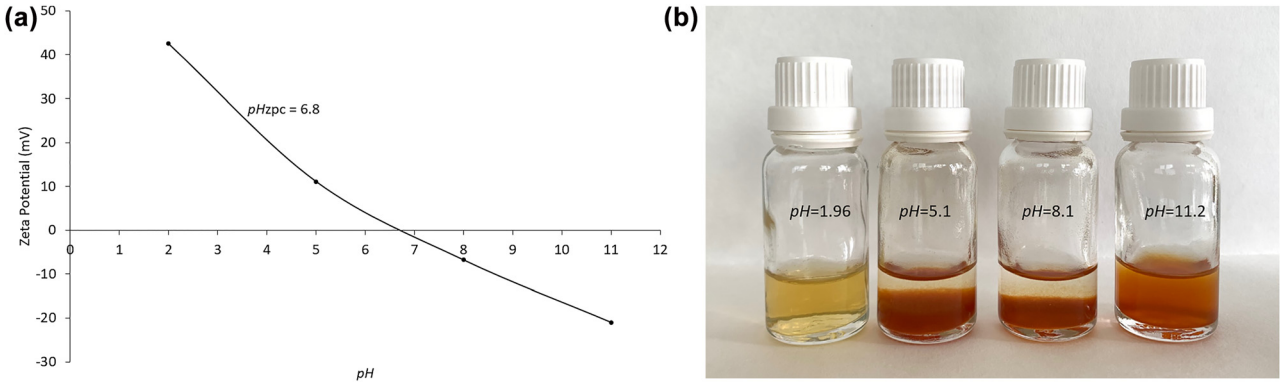

Figure 8: (a) Zeta potential versus *pH* plot for colloidal gIONPs, and (b) images of gIONPs colloidal solution at different *pH* values.

3.4 Antibacterial activity evaluation of gIONPs

The Agar well diffusion method was employed to evaluate the antibacterial activity of the powder form of gIONPs against the Gram-negative (*E. coli*) and Gram-positive (*S. aureus)* bacteria species. gIONPs showed clear zones of inhibition of 24.27 ± 0.12 mm and 20.83 ± 0.11 mm in 250 mg/mL concentration against *S. aureus* and *E. coli* bacteria respectively. The negative control of *C. siliqua L.* (carob pod) extract did not affect microbial growth whereas the standard antibiotics selected as positive control showed inhibition on the selected microorganisms. The inhibition activity of the gIONPs was compared with standard antibiotics Cefoxitin, Cefotaxime, Gentamicin, and Tetracycline as shown in Table 5. The results were compared with the standard Kirby–Bauer interpretation chart (Table S2). The Gram-positive bacteria *S. aureus* were found to be more susceptible to gIONPs than the Gram-negative bacteria *E. coli*. gIONPs showed the highest inhibition zone against *S. aureus* when compared with 4 standard antibiotics. The antibacterial effect of gIONPs showed a greater inhibition activity against *S. aureus* than *E. coli* bacteria (Figure 9). This might be because of the differences in the cell wall composition of bacteria [63].

The inhibitory action of gIONPs may be attributed to the oxidative stress by reactive oxygen species generation and the Fenton reaction [64]. When iron nanoparticles penetrate cells through disrupted membranes, it may cause further damage. Li et al. [65] found that the iron oxide nanoparticles not only inhibited *E. coli* cell growth, but also caused bacterial cell death due to the production of significantly elevated reactive oxygen species (ROS) such as hydroxyl radicals, superoxide radicals, and singlet oxygen, and hydrogen peroxide levels. Das et al. [66] performed the ROS measurement studies of *S. aureus* in presence of iron oxide nanoparticles. They found that iron oxide nanoparticles enhance the fluorescence intensity significantly which is directly correlated with the quantity of ROS developed in *S. aureus* bacterial cells. Similar results of the antibacterial effect of iron nanoparticles on *S. aureus* and *E. coli* have been reported in recent studies. Kanagasubbulakshmi and Kadirvelu [67] evaluated the antibacterial property of iron oxide nanoparticles against Gram-negative – *E. coli* and Gram-positive – *S. aureus*. They found the zone of inhibition of 10 mm and 8 mm for *E. coli* and *S. aureus*, respectively. Suganya et al. [68] reported the considerable antibacterial activity of iron oxide nanoparticles from leaf extract of *Passiflora foetida*

Table 5: Zone inhibition of gIONPs, *Ceratonia siliqua L.* (carob pod) extract, and standard antibiotics against selected bacterial strains.

	Zone of Inhibition (Diameter in mm)	
	S. aureus	***E. coli***
Ceratonia siliqua L. extract	–	–
Cefoxitin (FOX) (30 µg/disc)	11.87 ± 0.14	28.46 ± 0.11
Cefotaxime (CTX) (30 µg/disc)	–	14.27 ± 0.09
Gentamicin (CN) (10 µg/disc)	23.62 ± 0.16	22.83 ± 0.08
Tetracycline (TE) (30 µg/disc)	10.5 ± 0.15	23.92 ± 0.14
gIONPs (250 mg/mL)	24.27 ± 0.12	20.83 ± 0.11

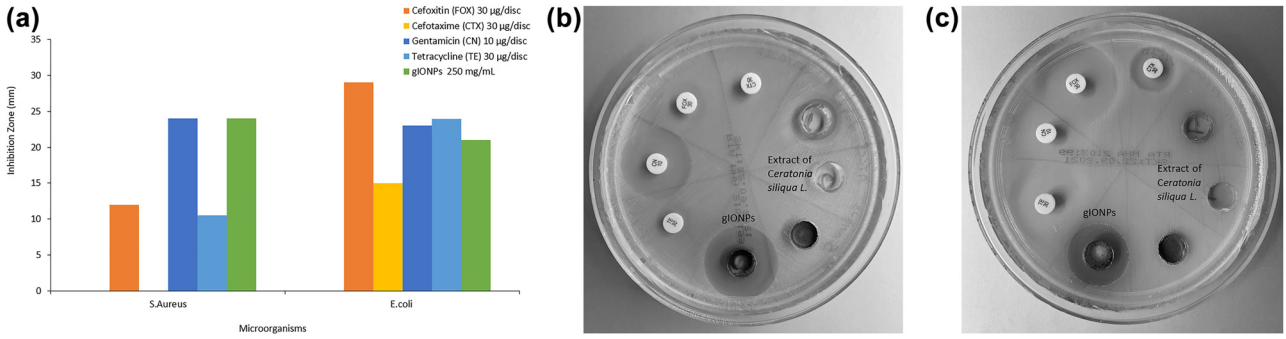

Figure 9: (a) Antibacterial activity of gIONPs, *Ceratonia siliqua L.* (carob pod) extract, and standard broad-spectrum antibiotics (Cefoxitin (FOX), Cefotaxime (CTX), Gentamicin (CN), and Tetracycline (TE)) against *S. aureus* and *E. coli* bacteria (b) and (c) the plates showing the inhibition zones of gIONPs and *Ceratonia siliqua L.* (carob pod) extract, and standard broad-spectrum antibiotics (Cefoxitin (FOX), Cefotaxime (CTX), Gentamicin (CN), and Tetracycline (TE)) against *S. aureus* and *E. coli* bacteria.

towards Gram-negative and positive bacteria. They found the zone of inhibition for *S. aureus* and *E. coli* to be 11 mm and 18 mm, respectively.

4 Conclusions

This study focused on the optimization of the green synthesis parameters for the stable colloidal form of gIONPs and evaluation of the antibacterial effect of the gIONPs powder against Gram-negative (*E. coli*) and Gram-positive (*S. aureus*) bacteria.

The synthesis parameters at the optimum values produced monodispersed and spherical iron oxide nanoparticles of the hydrodynamic size of around 78 ± 22 nm due to the availability of reducing, stabilizing, and capping biomaterials from *C. siliqua L.* (carob pod) aqueous extract. Reaction time and temperature were the most effective parameters in the monodisperse iron oxide nanoparticle synthesis reaction. By producing monodisperse iron oxide nanoparticles, the low total surface free energy of the system was maintained and the state of the system became stable. The particles were effectively surrounded by biomaterials from *C. siliqua L.* (carob pod) aqueous extract without any external addition of surfactant and polymers The stability of the iron oxide nanoparticles was preserved for 3 months at +41 ± 0.8 mV by only optimizing the synthesis parameters. Nanomaterials stabilization is enhancing their usefulness in sensors, biomedical devices, and electronics applications. The high zeta potential is a helpful sign of long storage. Therefore, this study has novelty in terms of maintaining the stability of iron oxide nanoparticles by only optimizing the synthesis parameters in terms of ease of fabrication and material minimalism. Further, the powder form of these iron oxide nanoparticles at 98 ± 15 nm size showed antibacterial activity against both Gram-negative (*E. coli*) and Gram-positive (*S. aureus*) bacteria. The gIONPs inhibited the growth of *S. aureus* with high susceptibility when compared with the standard antibiotics of Cefotaxime, Tetracycline, Gentamicin, and Cefoxitin and also the growth of *E. coli* when compared with the standard antibiotics of Tetracycline and Gentamicin. gIONPs could serve as a potential antibacterial agent. Understanding the interactions at the nanomaterial and biological interface helps in implementing approaches for the use of iron oxide nanomaterials in the biomedical, clinical, and pharmaceutical industries.

Author contribution: Derya Aksu Demirezen: Methodology, Data curation, Investigation, Writing - original draft. Şeyda Yılmaz: Methodology, Data curation. Dilek Demirezen Yılmaz: Methodology, Resources. Yalçın Şevki Yıldız: Resources, Funding.

Research funding: This study was financially supported by the Erciyes University Scientific Research Projects Coordination department with a project number of FDK−2021−10896.

Conflict of Interest: The authors declare that they have no known competing financial interests or personal relationships that could have appeared to influence the work.

References

1. Ray T. R., Lettiere B., Rutte J. D., Pennathur S. *Langmuir* 2015, *31*, 3577−3586. https://doi.org/10.1021/la504511j.
2. Singh J., Dutta T., Kim K., Rawat M., Samddar P., Kumar P. *J. Nanobiotechnol.* 2018, *16*, 1−24. https://doi.org/10.1186/s12951-018-0408-4.
3. Herlekar M., Barve S., Kumar R. *J. Nanoparticle Res.* 2014, *2014*, 140614. https://doi.org/10.1155/2014/140614.

4. Patra J. K., Baek K. *J. Nanoparticle Res.* 2014, *2014*, 417305. https://doi.org/10.1155/2014/417305.
5. Nene A., Takahashi K. W. M., Umeno M. J. *Nano Res.* 2016, *40*, 8–19. https://doi.org/10.4028/www.scientific.net/JNanoR.40.8.
6. Krishnamoorthi R., Bharathakumar S., Malaikozhundan B., Mahalingam P. U. *Biocatal. Agric. Biotechnol.* 2021, *35*, 102107. https://doi.org/10.1016/j.bcab.2021.102107.
7. Ajinkya N., Yu X., Kaithal P., Luo H., Somani P., Ramakrishna S. *Materials* 2020, *4644*, 13. https://doi.org/10.3390/ma13204644.
8. Kudr J., Haddad Y., Richtera L., Heger Z., Cernak M., Adam V., Zitka O. *Nanomaterials* 2017, *7*, 243. https://doi.org/10.3390/nano7090243.
9. Feng Q., Liu Y., Huang J., Chen K., Huang J., Xiao K. *Sci. Rep.* 2018, *2082*, 1–13. https://doi.org/10.1038/s41598-018-19628-z.
10. Li W., Liu D., Wu J., Kim C., Fortner J. D. *Environ. Sci. Technol.* 2014, *48*, 11892–11900. https://doi.org/10.1021/es502174p.
11. Thukkaram M., Sitaram S., Kannaiyan S. K. *Int J Biomater* 2014, *2014*, 716080. https://doi.org/10.1155/2014/716080.
12. Ayaz F. A., Torun H., Ayaz S., Correira P. J., Alaiz M., Sanz C., Grux J., Strnad M. *J. Food Qual.* 2007, *30*, 1040–1055. https://doi.org/10.1111/j.1745-4557.2007.00176.x.
13. Gökkuş Ö., Yıldız N., Koparal A. S., Yıldız Y. Ş. *Int. J. Environ. Sci. Technol.* 2018, *15*, 449–460. https://doi.org/10.1007/s13762-017-1404-1.
14. Aksu Demirezen D., Demirezen Yılmaz D. *Inorg. Nano-Met. Chem.* 2021, *52*, 761–771. https://doi.org/10.1080/24701556.2021.1980032.
15. Aksu Demirezen D., Yıldız Y. Ş., Demirezen Yılmaz D. *J. Biosci. Bioeng.* 2019, *127*, 241–245. https://doi.org/10.1016/j.jbiosc.2018.07.024.
16. Wiese G. R., Healy T. W. *J. Chem. Soc. Faraday Trans.* 1970, *66*, 490–499. https://doi.org/10.1039/TF9706600490.
17. Aisida S. O., Madubuonu N., Alnasir M. H., Ahmad I., Botha S., Ezema F. I. *Appl. Nanosci.* 2020, *10*, 305–315. https://doi.org/10.1007/s13204-019-01099-x.
18. Arasu M. V., Arokiyaraj S., Viayaraghavan P., Kumar T. S. J., Duraipandiyan V., Al-Dhabi N. A., Kaviyarasu K. *J. Photochem. Photobiol. B Biol.* 2019, *190*, 154–162. https://doi.org/10.1016/j.jphotobiol.2018.11.020.
19. Nwanya A. C., Razanamahandry L. C., Bashir A., Ikpo C. O., Nwanya S. C., Botha S., Ntwampe S. K. O., Ezema F. I., Iwuoha E. I., Maaza M. *J. Hazard Mater.* 2019, *375*, 281–289. https://doi.org/10.1016/j.jhazmat.2019.05.004.
20. Aisida S. O., Ugwu K., Akpa P. A., Nwanya A. C., Ejikeme P. M., Botha S., Ahmad I., Maaza M., Ezema F. I. *Mater. Chem. Phys.* 2019, *237*, 121859. https://doi.org/10.1016/j.matchemphys.2019.121859.
21. Aisida S. O., Ugwu K., Akpa P. A., Nwanya A. C., Nwankwoa U., Botha S. S., Ejikeme P. M., Ahmad I., Maaza M., Ezema F. I. *Surface. Interfac.* 2019, *17*, 100359. https://doi.org/10.1016/j.surfin.2019.100359.
22. Aksu Demirezen D., Yılmaz Ş., Demirezen Yılmaz D. *IJASEAT* 2018, *6*, 25–29.
23. Danaei M., Dehghankhold M., Ataei S., Davarani F. H., Javanmard R., Dokhani A., Khorasani S., Mozafari M. R. *Pharmaceutics* 2018, *10*, 57. https://doi.org/10.3390/pharmaceutics10020057.
24. Ramimoghadam D., Bagheri S., Hamid S. B. A. *Colloids Surf., B* 2015, *133*, 388–411. https://doi.org/10.1016/j.colsurfb.2015.02.003.
25. Tahir K., Nazir S., Baoshan L., Khan A. U., Khan Z. U. H., Ahmad A., Khan F. U. *Separ. Purif. Technol.* 2015, *150*, 316–324. https://doi.org/10.1016/j.seppur.2015.07.012.
26. Hamouda R. A., Hussein M. H., Abo-elmagd R. A., Bawazir S. *Sci. Rep.* 2019, *9*, 13071. https://doi.org/10.1038/s41598-019-49444-y.
27. Junaidi M. Y., Harsojo E. S., Kuwat T. *Int. J. Adv. Sci. Eng. Inf. Technol.* 2016, *6*, 365–369. https://doi.org/10.18517/ijaseit.6.3.808.
28. Kartini K., Alviani A., Anjarwati D., Fanany A. F., Sukweenadhi J., Avanti C. *Processes* 2020, *8*, 998. https://doi.org/10.3390/pr8080998.
29. Saxena J., Sharma P. K., Sharma M. M., Singh A. *SpringerPlus* 2016, *5*, 861. https://doi.org/10.1186/s40064-016-2558-x.
30. Satpathy S., Patra A., Ahirwar B., Hussain M. D. *Physica E* 2020, *121*, 113830. https://doi.org/10.1016/j.physe.2019.113830.
31. Ahmed S., Saifullah, Ahmad M., Swami B. L., Ikram S, *J. Radiat. Res. Appl. Sci.* 2016, *206*, 1–7. https://doi.org/10.1016/j.jrras.2015.06.006.
32. Kheshtzar R., Berenjian A., Taghizadeh S. M., Ghasemi Y. *Green Process. Synth.* 2019, *8*, 846–855. https://doi.org/10.1515/gps-2019-0055.
33. Gholami A., Khosravi R., Khosravi A., Samadi Z. *Data Brief* 2018, *21*, 1779–1783. https://doi.org/10.1016/j.dib.2018.11.030.
34. Bijarbooneh F. H., Zhao Y., Kim J. H., Sun Z., Malgras V., Aboutalebi S. H., Heo Y.-U., Ikegami M., Dou S. X. *J. Am. Ceram. Soc.* 2013, *96*, 2636–2643. https://doi.org/10.1111/jace.12371.
35. Patra J. K., Baek K. *J. Photochem. Photobiol., B* 2017, *173*, 291–300. https://doi.org/10.1016/j.jphotobiol.2017.05.045.
36. Njagi E. C., Huang H., Stafford L., Genuino H., Galindo H. M., Collins J. B., Hoag G. E., Suib S. L. *Langmuir* 2011, *27*, 264–271. https://doi.org/10.1021/la103190n.
37. Kumar B., Smita K., Cumbal L., Debut A., Galeas S., Guerrero V. H. *Mater. Chem. Phys.* 2016, *179*, 310–315. https://doi.org/10.1016/j.matchemphys.2016.05.045.
38. Takeda M., Onishi T., Nakakubo S., Fujimoto S. *Mater. Trans.* 2009, *50*, 2242–2246. https://doi.org/10.2320/matertrans.M2009097.
39. Maity D., Agrawal D. *J. Magn. Magn Mater.* 2007, *308*, 46–55. https://doi.org/10.1016/j.jmmm.2006.05.001.
40. Rosicka D., Sembera J. *Nanoscale Res. Lett.* 2013, *8*, 1–9. https://doi.org/10.1186/1556-276X-8-20.
41. Rahman S. S. U., Qureshi M. T., Sultana K., Rehman W., Khan M. Y., Asif M. H., Farooq M., Sultana N. *Results Phys.* 2017, *7*, 4451–4456. https://doi.org/10.1016/j.rinp.2017.11.001.
42. Gutiérrez L., de la Cueva L., Moros M., Mazarío E., de Bernardo S., de la Fuente J. M., Morales M. P., Salas G. *Nanotechnology* 2019, *30*, 112001. https://doi.org/10.1088/1361-6528/aafbff.

43. Femi-Adepoju A. G., Dada A. O., Otun K. O., Adepoju A. O., Fatoba O. P. *Heliyon* 2019, *5*, e01543. https://doi.org/10.1016/j.heliyon.2019.e01543.
44. Nikaeen G., Yousefinejad S., Rahmdel S., Samari F., Mahdavinia S. *Sci. Rep.* 2020, *10*, 9642. https://doi.org/10.1038/s41598-020-66357-3.
45. Guven B., Durakli-Velioglu S., Boyacı i. H. *Gıda* 2019, *44*, 274–290. https://doi.org/10.15237/gida.GD18119.
46. Rajiv P., Deepa A., Vanathi P., Vidhya D. *Int. J. Pharm. Pharmaceut. Sci.* 2017, *9*, 315–318. https://doi.org/10.22159/ijpps.2017v9i1.11053.
47. Coates J. Interpretation of infrared spectra, a practical approach. In *Encyclopedia of Analytical Chemistry*; Meyers R. A., McKelvy M. L., Eds. John Wiley & Sons, Ltd.: Hoboken, New Jersey, 2006.
48. Khan F. U., Chen Y., Khan N. U., Ahmad A., Tahir K., Khan Z. U., Khan A. U., Khan S. U., Raza M., Wan P. *Microb. Pathog.* 2017, *107*, 419–424. https://doi.org/10.1016/j.micpath.2017.04.024.
49. Trivedi M. K., Patil S., Shettigar H., Bairwa K., Jana S. *Chem. Sci. J.* 2015, *6*, 100098. https://doi.org/10.4172/2150-3494.100098.
50. Hou Y., Hou C., Fan Y., Dang F., Li B. W. *Mater. Res. Express* 2017, *4*, 1–9. https://doi.org/10.1088/2053-1591/aa9e65.
51. Horn M., Nienhaus K., NienhausGerd U. N. *F1000Research* 2014, *3*, 290. https://doi.org/10.12688/f1000research.5836.2.
52. Camara F. B. G., Costa L. A., Fidelis G. P., Nobre L. T. D. B., Dantas-Santos N., Cordeiro S. L., Costa M. S. S. P., Alves L. G., Rocha H. A. O. *Mar. Drugs* 2011, *9*, 124–138. https://doi.org/10.3390/md9010124.
53. Mazumder A., Davis J., Rangari V., Curry M. *Int. Sch. Res. Notices* 2013, *2013*, 843709. https://doi.org/10.1155/2013/843709.
54. Rada S., Dehelean A., Culea E. *J. Mol. Model.* 2011, *17*, 2103–2111. https://doi.org/10.1007/s00894-010-0911-5.
55. Das A. K., Marwal R. V. A. *NH* 2014, *7*, 69–86. https://doi.org/10.4028/www.scientific.net/NH.7.69.
56. Lu W., Shen Y., Xie A., Zhang W. J. *Magn. Magn. Mater.* 2010, *322*, 1828–1833. https://doi.org/10.1016/j.jmmm.2009.12.035.
57. Mahajan A., Ramana E. V. *Recent Pat. Mater. Sci.* 2014, *7*, 109–130. https://doi.org/10.2174/1874464807666140701190424.
58. Aksu Demirezen D., Yıldız Y. Ş., Demirezen Yılmaz D. *Environ. Nanotechnol. Monit. Manag.* 2019, *11*, 100219. https://doi.org/10.1016/j.enmm.2019.100219.
59. Kovář D., Malá A., Mlčochová J., Kalina M., Hlaváček Z. F., Antonín H., Farka Z., Skládal P., Starčuk Z., Jiřík R., Slabý O., Hubálek J. *J. Nanomater.* 2017, *2017*, 7859289. https://doi.org/10.1155/2017/7859289.
60. El-Brolossy T. A., Abdallah T., Mohamed M. B., Abdallah S., Easawi K., Negm S., Talaat H. *Eur. Phys. J. Spec. Top.* 2008, *153*, 361–364.
61. Huong V. T. L., Thang N. N. *Mater. Today Proc.* 2021, *42*, 88–93. https://doi.org/10.1016/j.matpr.2020.10.015.
62. Shoaib M., Naz A., Osra F. A., Abro S. H., Qazi S. U., Siddiqui F. A., Shah M. R., Mirza A. Z. *Arab. J. Chem.* 2021, *14*, 102974. https://doi.org/10.1016/j.arabjc.2020.102974.
63. Guzman M. G., Dille J., Godet S. *Nanomed.: Nanotechnol. Biol. Med.* 2012, *8*, 37–45. https://doi.org/10.1016/j.nano.2011.05.007.
64. Mohamed Y. M., Azzam A. M., Amin B. H., Safwat N. A. *Afr. J. Biotechnol.* 2015, *14*, 1234–1241. https://doi.org/10.5897/AJB2014.14286.
65. Li Y., Yang D., Wang S., Li C., Xue B., Yang L., Shen Z., Jin M., Wang J., Qiu Z. *Molecules* 2018, *23*, 602. https://doi.org/10.3390/molecules23030606.
66. Das S., Diyali S., Vinothini G., Perumalsamy B., Balakrishnan G., Ramasamy T., Dharumadurai D., Biswas B. *Heliyon* 2020, *6*, e04953. https://doi.org/10.1016/j.heliyon.2020.e04953.
67. Kanagasubbulakshmi S., Kadirvelu K. *Def. Life Sci. J.* 2017, *2*, 422–427. https://doi.org/10.14429/dlsj.2.12277.
68. Suganya D., Rajan M. R., Ramesh R. *Int. J. Curr. Res.* 2016, *8*, 42081–42085. https://doi.org/10.22159/ajpcr.2017.v10i4.15744.

Supplementary Material: The online version of this article offers supplementary material (https://doi.org/10.1515/ijmr-2022-0037).